Academic Journal of Science and Technology
ISSN: 2771-3032 | Vol. 21, No. 1, 2026

Study on Laser Additive Joining Process of Stainless Steel and Copper Alloy

Weihao Chen, Senpeng Fang, Luchen Wei, Shixiang Cheng, Shaoting Cao

AVIC Chengdu Aircraft Industrial (Group)Co.,Ltd, Chengdu 610092, China

Abstract: This study achieved the joining of 316 stainless steel and T3 copper using a laser additive joining method. The process feasibility of using pure 316 stainless steel powder and pure copper powder as filler materials for additive joining was investigated, and the influence of different joining processes on the microstructure evolution and mechanical properties of the joints was analyzed. The research indicates that when pure 316 powder is used as the filler material, with a laser heating power of 1.8 kW on the steel side and 2.2 kW on the copper side, the joint formation is optimal, and the tensile strength of the joint reaches 250.3 MPa. When pure copper powder is used as the joining material, the internal stress within the joint is relatively large, and aging fracture occurs in the transition zone on the copper side.

Keywords: Laser additive joining; Steel and copper; Microstructure; Mechanical properties.

1. Introduction

Copper possesses excellent thermal and electrical conductivity. Due to its chemically inactive nature, it exhibits good corrosion resistance in ordinary atmospheric environments. However, because of its low mechanical strength, it is not suitable for direct use as a structural material and is often employed in the manufacture of wires, thermal conductive materials, and corrosion-resistant devices [1-5]. Stainless steel typically contains elements such as Cr, Ni, Mn, and Mo, making it a high-alloy steel with high chemical stability. Stainless steel offers good oxidation resistance, corrosion resistance, and excellent mechanical properties, making it suitable for manufacturing components and equipment requiring high corrosion resistance, strong oxidation resistance, and high-temperature endurance [6-8]. Nevertheless, single copper alloys or stainless steels can hardly meet the ever-growing demands of modern production or satisfy specific engineering requirements. In recent years, functionally graded materials combining copper and stainless steel have garnered increasing attention from researchers worldwide, and the welding of copper and stainless steel has become a focal point of research.

This research is primarily based on the principle of laser solid forming and investigates the laser additive joining process for T3 copper and 316 austenitic stainless steel. It analyzes the microstructural characteristics and their evolution when introducing different filler materials. Based on the analysis of the microstructure and mechanical property test results, the study explores the influence of different filler materials on the properties of additively joined components between T3 copper and 316 stainless steel.

The difficulty in joining copper and steel in this experiment lies in their significant differences in thermal conductivity, physical properties, and linear expansion coefficients. Furthermore, the phenomenon of liquid phase separation between Fe and Cu makes it difficult to obtain a good joint using conventional fusion welding methods. The transition layer has a decisive influence on the joint's performance. By adjusting the ratio of copper powder to 316 powder in the transition layer, different joining layers are obtained, and the microstructure under these various joining layers is subsequently analyzed.

Prior to the main experiment, preliminary tests were conducted to determine the optimal joining parameters, such as laser power, powder feed rate, and welding speed, for joining copper and steel with different powder ratios. Subsequently, the optimal parameters for the different processes were used to join T3 copper and 316 austenitic stainless steel. Finally, the microstructure of the base materials and the weld zone after joining was analyzed to compare the effects of different joining processes on the microstructure of the T3 copper and 316 stainless steel base materials and the weld zone.

2. Experimental Materials and Test Plan

2.1. Experimental Materials

The base materials selected for this experiment were T3 copper and 316 stainless steel. T3 copper is industrially defined as pure copper but contains trace amounts of alloying elements, with a Cu content exceeding 99.5%; it is sometimes also referred to as a copper alloy. 316 austenitic stainless steel belongs to the 18-10 series of austenitic stainless steels, with Fe as the matrix element, incorporating over ten elements including Cr and Mo (the chemical composition is shown in Table 2-1). The dimensions of both materials were 70.00 mm × 50.00 mm × 7 mm.

Table 2-1. Chemical composition of 316 austenitic stainless steel (wt.%)

C	Mn	P	S	Ni	Cr	Mo
<0.08	<2	<0.045	<0.03	10.0-14.0	16.0-18.0	2.00-3.00

The main equipment used in this experiment included a powder drying oven, a powder feeding device, a shielding gas

system, a welding system, a welding control system, and a cooling system. Before the test, an SZG powder dryer was used to dry the copper powder and 316 powder to reduce the impact of moisture on welding quality. The test substrates were T3 copper and 316 stainless steel plates with dimensions of 70.00 mm × 50.00 mm × 7 mm. Process parameters for powder spreading were first investigated on the 316 and T3 copper plates. Initially, single tracks were deposited on the 316 stainless steel plate surface using pure 316 powder and 50 wt.% pure copper powder sequentially to study the forming effect of different powder ratios on the 316 steel plate.

2.2. Microstructure Observation

The groove of the laser additively joined component was machined. A milling machine was used to flatten the weld reinforcement on the groove surface. The sample was then cut using wire electrical discharge machining (WEDM) to dimensions of 20 mm × 5 mm × 5 mm. After mounting, the specimens were ground sequentially using 240#, 800#, 1500#, 2000#, and 3000# abrasive papers. Polishing was performed using diamond abrasive pastes with particle sizes of W2.5 and W1. Since the surface hardness of annealed stainless steel is higher than that of T3 copper, after polishing with the W2.5 paste, a further polishing step using W1 paste was applied specifically to the copper surface.

3. The Application of Traditional Embroidery Art in Modern Fashion Design

3.1. Macroscopic Morphology Analysis of Welded Joints

Figure 3-1 shows the macroscopic morphology of the welded joints under three different processes. Figure 3-1(a) shows the macroscopic morphology of the joint filled with pure copper powder. During the wire cutting process, the joint filled with pure copper powder experienced failure fracture in the transition zone between the copper base material and the weld. Due to the high reflectivity of copper to the laser, a higher laser heating power was used, which increased the wetting and spreadability of liquid copper. However, significant heat accumulation, combined with external constraints on the copper base material, readily leads to the accumulation of structural stress and thermal stress. This resulted in crack propagation at the interface junction, leading to failure fracture.

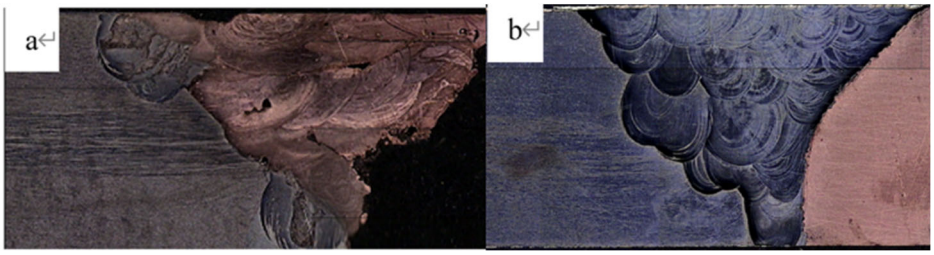

Figure 3-1. Macroscopic morphology of joints under different process parameters

(a) Macroscopic morphology of the joint filled with copper powder; (b) Macroscopic morphology of the joint filled with 316 powder;

Figure 3-1(b) shows the joint made with 316 powder. The joint overall exhibits good integrity, with no obvious surface cracks, lack of fusion, or other defects. Due to the low thermal conductivity and high linear expansion coefficient of the steel side, the heat-affected zone on the steel side expands continuously under prolonged heating. Macroscopically, this manifests as the fusion zone on the steel side displaying a morphology distributed from the middle to the upper part of the joint. At the bottom of the copper side, due to relatively small initial heat accumulation, the heat input has a lesser impact on the base material and weld, and a fine keyhole effect structure can be observed macroscopically. The weld center corresponds to multi-layer, multi-pass welding, but due to copper's good thermal conductivity, no burning phenomenon is observed macroscopically.

3.2. Microstructural Analysis of Joints

3.2.1. Microstructural Analysis of Joints Made with Pure Copper Powder

When using pure copper powder for additive joining, the weld was intact after filling the groove, with no obvious pores or cracks observed macroscopically. At the bottom of the copper-side weld, a spherical pore could be clearly observed under an optical microscope. This pore may have formed because the copper cooling rate was high at the initial stage of powder feeding. Oxidation of copper in the weld generated cuprous oxide, which reacted with the liquid metal in the molten pool to produce water vapor insoluble in the liquid metal. Under rapid cooling conditions, this water vapor could not escape from the weld in time, forming the pore. Due to the protection of triple argon shielding, the oxygen content around the workpiece was extremely low (<100 ppm), resulting in few pores in the weld. In the metallographic image shown in Figure 3-2, the weld microstructure is fine and dense, but obvious cracks are present. The crack likely originated from the pore, where stress concentration formed. Under continuous heat input accumulation, thermal stress increased continuously, leading to cracking at the pore location.

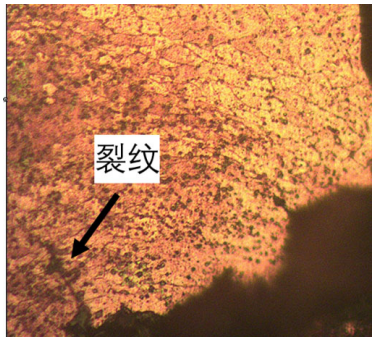

Figure 3-2. Metallographic structure of the copper-side weld

Compared to the interface joining on the copper side, the joining on the 316 stainless steel side was better. Under the metallographic microscope, the interface joining on the steel side was dense, with no obvious cracks or pores. At low magnification under the optical microscope, the overall weld morphology appeared favorable, with lack of fusion occurring only at a few locations. At high magnification, a small amount of lack of fusion could be observed in the upper part of the weld, forming distinct cracks.

3.2.2. Microstructural Analysis of Joints Made with Pure 316 Stainless Steel Powder

Filling the groove with pure 316 stainless steel powder resulted in better weld quality compared to using pure copper powder. The weld surface had no obvious cracks or pores. The interface junction on the steel side was superior to that on the copper side, with no apparent lack of fusion on the steel side, while some lack of fusion existed on the copper side. The weld grains were fine, and no metallurgical defects appeared in the center of the weld. However, a small amount of lack of fusion was observed near the fusion line close to the copper side. This might be because a small amount of 316 powder adhered to the copper side during laser heating, causing significant reflection of laser heat, which prevented the melting of some 316 powder particles and left metallurgical defects in certain areas. A small number of black particles were present on the weld surface. Energy dispersive spectroscopy (EDS) analysis of these black particles revealed that they primarily contained Fe and Mn elements. Based on the Cu-Fe binary phase diagram and EDS results, the black particles were mainly Fe-rich α-phase. Figure 3-3(a) is a scanning electron microscope (SEM) image of the weld, and Figure 3-3(b) shows the corresponding EDS elemental analysis. The EDS results indicate that the main component of the weld is 316 stainless steel, with almost no diffusion of Cu into the weld. This is because Cu and Fe have only limited mutual solubility in the solid state. Furthermore, due to the small heat input and relatively low weld temperature during laser heating, the diffusion coefficient of the Cu element is small and diffusion is slow; thus, the weld contained virtually no Cu element.

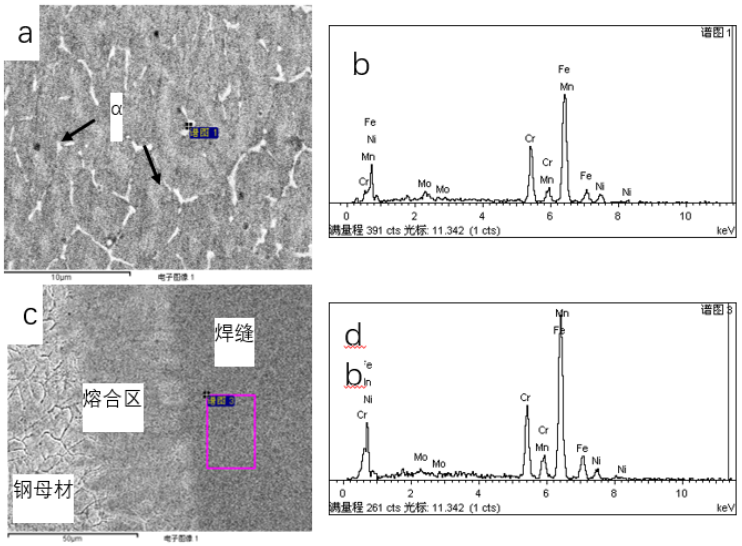

Figure 3-3. Microstructure of the weld made with pure 316 powder
(a) α-phase at the steel-side interface; (b) EDS analysis of the α-phase;
(c) SEM image of the steel side; (d) EDS analysis of the steel-side weld

The scanning electron micrograph in Figure 3-5(c) shows that the connection on the steel side is divided into three zones: the fusion zone of the weld, the transition zone between the steel and the weld, and the steel base material. Under the scanning electron microscope, the transition zone exhibits fine grains and contains relatively high amounts of Mn and Cr elements. Mn can enhance the crack resistance of grain boundaries, while Cr can improve their corrosion resistance. Consequently, no cracks were observed under the optical or scanning electron microscopes, and the etchant had a weak effect on the center of the fusion zone. In contrast to the interface joining on the steel side, the copper-side interface showed distinct metallurgical defects. Under the optical microscope, the copper-side interface was well-connected but contained a small number of metallurgical defects.

Lack of fusion occurred in the middle-lower position of the copper-side fusion zone. This location likely suffered from insufficient heat accumulation, with the laser heating energy being largely reflected, preventing the 316 powder from melting and causing it to adhere to the surface of the copper plate substrate. Scanning electron microscopy revealed a large number of black particulate phases. EDS analysis indicated that these black particulate phases were not metallurgical defects. The black particulate phase contained 52.27% Fe, 34.24% Cu, and 13.48% Cr. Therefore, it is inferred that the black particulate phase is neither porosity nor lack of fusion but rather corrosion pits formed on the copper matrix due to etchant attack, appearing as black particulate phases. The EDS analysis results of the copper-side weld show that the weld contains a large amount of alloying elements such as Ni, Mo, and Cr. The weld zone contained 18.25% Cr, an element that can enhance corrosion resistance; hence, no cracks or corrosion pits were found in the weld zone. Mo is a grain-refining element, and the copper-side weld contained 3.0% Mo, resulting in observably finer grains in the weld zone compared to the copper base material. In the liquid state, Ni can form infinite solid solutions with Fe and Cu. The bonding between grains is tight, with no obvious boundaries

visible under the electron microscope. Figure 3-4 shows the EDS line scan analysis across the copper-side weld.

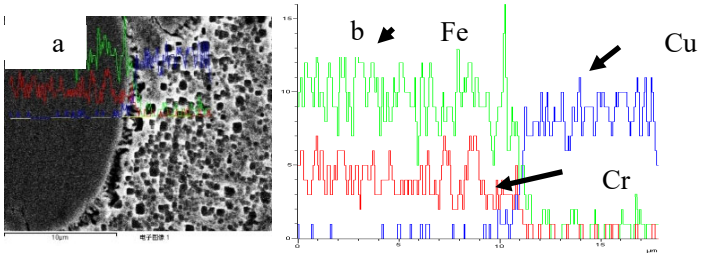

Figure 3-4. EDS line scan analysis of the copper-side weld
(a) SEM line scan across the copper side; (b) SEM analysis from line scan

3.3. Tensile Property Analysis of Joints

The tensile properties of a joint reflect its service performance. Analyzing the fracture causes of specimens prepared using different processes, based on weld microstructure, helps identify a suitable Cu-to-steel fusion ratio and appropriate process parameters, thus guiding the development of a reasonable welding process. For the specimen filled with pure 316 powder, tensile test results showed a joint tensile strength of 250.3 MPa, which is roughly equivalent to the tensile strength of the T3 copper base material (210.4 MPa), while the elongation was only 8%. Tests indicated that the elongation of the 316 base material is 30%, and its tensile strength is 485.0 MPa.

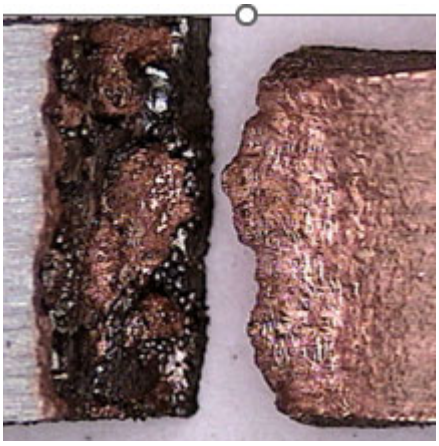

Figure 3-5. Macroscopic fracture morphology of the specimen filled with 316 powder

The macroscopic fracture morphology shows that the specimen joint fractured at the interface between the copper side and the weld, with significant necking observed on the copper side, while the fracture near the weld interface was brittle. In the copper-side microstructure shown in Figure 3-5, partial lack of fusion in the copper-side transition zone acted as potential crack sources. Under applied tensile force, internal cracks propagated continuously. The relatively large heat input coarsened the microstructure on the steel side, which to some extent reduced the tensile strength of the joint. Additionally, the transition zone on the copper side contained a large amount of α-phase, a hard and brittle phase that reduces both joint toughness and tensile strength. Therefore, the macroscopic fracture of the joint manifests as ductile fracture on the copper side and brittle fracture in the transition zone.

When pure 316 powder was used as the filler material, with a laser heating power of 1.8 kW on the steel side and 2.2 kW on the copper side, the joint formation was optimal, achieving a tensile strength of 250.3 MPa, though the joint toughness was relatively poor. Joints produced using pure copper powder as the filler material exhibited high internal stress, resulting in aging fracture in the transition zone on the copper side.

4. Conclusion

In this study, laser additive joining processes for T3 copper and 316 stainless steel were investigated using pure 316 stainless steel powder and pure T3 copper powder. Through the analysis of the microstructure and mechanical properties of joints obtained via different joining processes, the following conclusions were drawn:

(1) Joining of 316 stainless steel and T3 copper using pure copper powder at a laser power of 3 kW resulted in poor joint formation. The joint exhibited a small number of cracks in the steel-side transition zone and significant lack of fusion in the copper-side transition zone. The specimen underwent aging fracture during machining, with the fracture occurring at the interface between the copper side and the base material.

(2) Joining 316 stainless steel and T3 copper using 316 powder resulted in a well-formed joint with a fine, dense microstructure. The tensile strength of the weld reached that of the T3 copper base material, with the joint exhibiting a tensile strength of 250.3 MPa. Tensile test fracture occurred at the interface of the transition zone between the copper base material and the weld, with relatively poor elongation of 8.2%.

References

[1] Xing, L. (2007). Microstructure analysis of low carbon steel and red copper friction stir welding joint. *Chinese Journal of Welding*, *28*(2), 17-20.

[2] Mai, T. A., & Spowage, A. C. (2004). Characterisation of dissimilar joints in laser welding of steel-kovar, copper-steel and copper-aluminium. *Materials Science and Engineering A*, *374*(1-2), 224-233.

[3] Hongwei, S., & Gupta, M. C. (2004). Nd: yttritium-aluminum-garnet laser welding of copper to stainless steel. *Journal of Laser Applications*, *16*(5), 2-8.

[4] Sun, Z. (1993). Laser beam welding of austenitic-ferrite dissimilar steel joints using nickel based filler wire. *Materials Science and Technology*, *19*, 603-608.

[5] Dawes, C., & Eng, C. (1998). Analysis of the explosive cladding of Cu–low carbon steel plates. Laser Welding, 16-18.

[6] Nishi, H., & Kikuchi, K. (1998). Influence of brazing conditions on the strength of brazed joints of dispersion-strengthened copper to 316 stainless steel. *Journal of Nuclear Materials*, *258-263*, 281-288.

[7] Carroll, B. E., Otis, R., et al. (2016). Functionally graded material of 304L stainless steel and Inconel 625 fabricated by directed energy deposition: characterization and thermodynamic modeling. *Acta Materialia*, *108*, 46-54.

[8] Phillips, R. H. (1992). Laser beam welding of HY80 and HY100 steels using hot welding wire addition. *Welding Journal*, *15*(7), 201-208.